

---

# Exploration of electrospinning hemp/polyacrylonitrile composite fiber membrane and dye adsorption capabilities

---

---

Received: 20 August 2025

---

Accepted: 18 December 2025

---

Published online: 09 February 2026

---

Cite this article as: Sun Y., Wang J., Kong W. *et al.* Exploration of electrospinning hemp/polyacrylonitrile composite fiber membrane and dye adsorption capabilities. *Sci Rep* (2026). <https://doi.org/10.1038/s41598-025-33369-w>

**Ying Sun, Jiayi Wang, Weishuai Kong & Yucan Jia**

---

We are providing an unedited version of this manuscript to give early access to its findings. Before final publication, the manuscript will undergo further editing. Please note there may be errors present which affect the content, and all legal disclaimers apply.

If this paper is publishing under a Transparent Peer Review model then Peer Review reports will publish with the final article.

# Exploration of Electrospinning Hemp/Polyacrylonitrile Composite Fiber Membrane and Dye Adsorption Capabilities

Ying Sun<sup>1,2,\*</sup>, Jiayi Wang<sup>1</sup>, Weishuai Kong<sup>1</sup> and Yucan Jia<sup>1</sup>

1: College of Light Industry and Textile, Qiqihar University, 161000, China.

2: Engineering Research Center for Hemp and Product in Cold Region of Ministry of Education, Qiqihar University, 161000, China.

\*Corresponding author:

Engineering Research Center for Hemp and Product in Cold Region of Ministry of Education, Qiqihar University. School of Light Industry and Textile, Qiqihar University. No. 42 Cultural Street, Jianhua District, Qiqihar City, Heilongjiang Province, Postal code 161000.

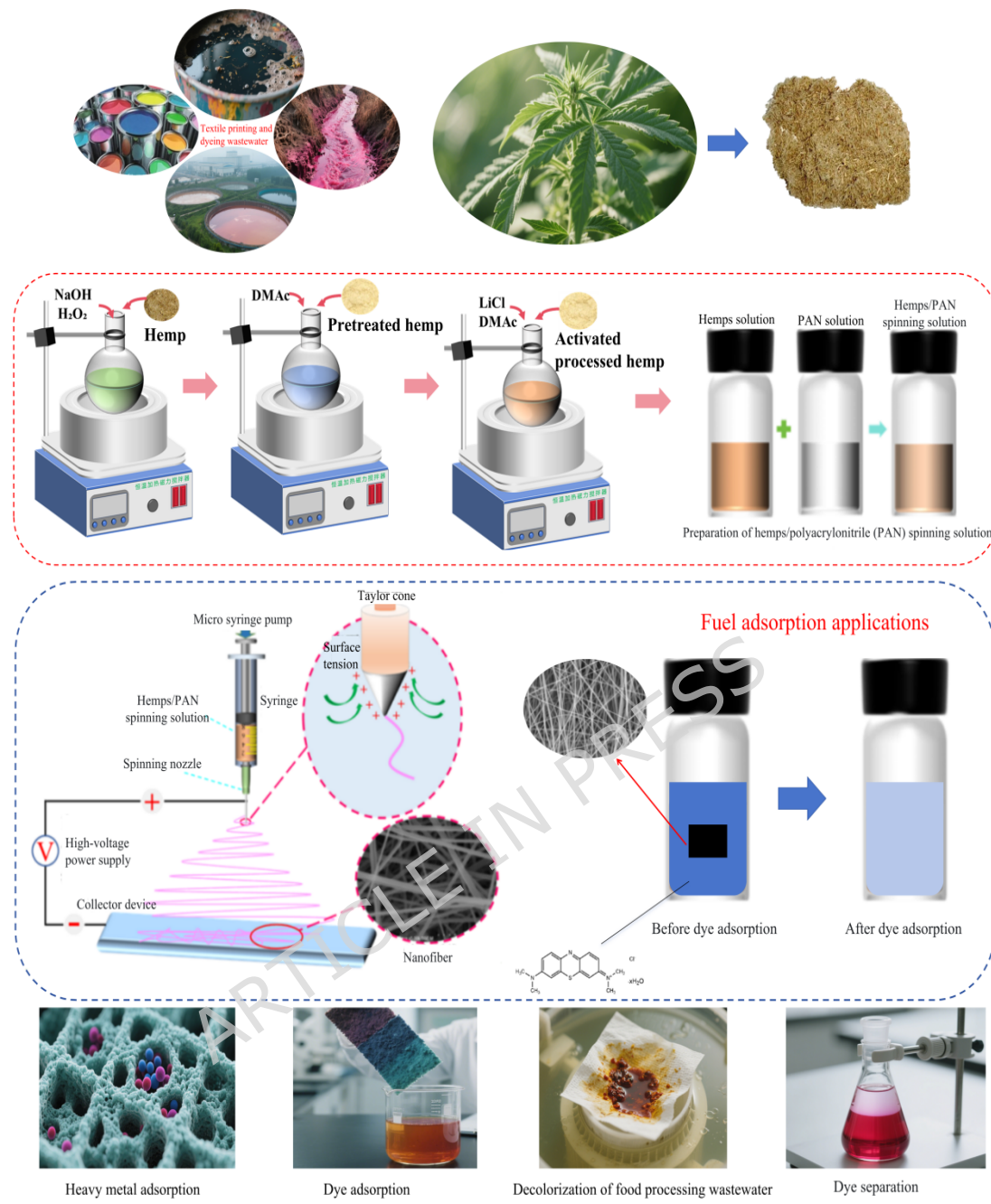
tel: 13803616812

E-mail: [sunying71750@sina.com](mailto:sunying71750@sina.com)

**Abstract:** Textile printing and dyeing wastewater has complex water quality and causes great harm. As a common pollutant, the cationic methylene blue dye is harmful to health. Therefore, adsorption technology plays a crucial role in wastewater treatment. To study the application of hemp/polyacrylonitrile nanocomposite fiber membranes in dye adsorption, this study employed electrospinning technology. This study used electrospinning to prepare hemp/polyacrylonitrile nanocomposite fiber

membranes for dye adsorption. Hemp fibers were dissolved in LiCl/DMAc, blended with polyacrylonitrile solution, and electrospun after single - factor optimization. The results show that the hemp/polyacrylonitrile composite fiber membrane has a uniform diameter distribution, good hydrophilicity, and excellent mechanical and physical properties. The particulate matter filtration test reveals that the membrane's filtration efficiency can reach 99.97 %. The adsorption of methylene blue by the hemp/polyacrylonitrile composite fiber membrane is more consistent with the pseudo - second - order kinetic model and the Langmuir adsorption isotherm model, indicating that it is mainly dominated by chemical adsorption. The adsorption process is a spontaneous endothermic reaction, and a higher temperature is more conducive to adsorption, with an adsorption capacity of up to 75.85 mg/g. The simple method yielded membranes with excellent dye adsorption and particulate filtration performance.

**Keywords:** Hemp fibers; Polyacrylonitrile; Electrospinning; Membrane; Methylene blue



## 1. Introduction

With the continuous industrial development, a large volume of wastewater is generated in the textile printing and dyeing industry<sup>[1-3]</sup>. Textile printing and dyeing wastewater is notoriously difficult to degrade. Its organic matter content and water temperature are also elevated. Additionally, its pH value fluctuates significantly. Its harmful impacts mainly include polluting water bodies, contaminating soil and posing substantial risks to human health and ecological security<sup>[4-8]</sup>. Cationic methylene blue (MB) dye is one of the most prevalent pollutants in textile printing and dyeing wastewater. It exhibits excellent stability and reducibility. It is widely used for dyeing various materials, it can also stain biological tissues and bacterial cells, thereby endangering human health. Excessive exposure may lead to disorders of the digestive and nervous systems, and it also carries a certain carcinogenic risk<sup>[9]</sup>.

In the treatment of textile printing and dyeing wastewater, adsorption technology plays a crucial role. Adsorption technology has the advantage of effectively removing pollutants such as organic substances, chromaticity, and heavy metals in wastewater, which is beneficial for enhancing the overall treatment efficiency. Additionally it features simple operation, low equipment investment and reduced operation costs, demonstrating strong applicability in practical engineering<sup>[10,11]</sup>. Electrospinning technology enables the fabrication of nanofiber membranes with diverse structures and properties.

Electrospun nanofiber membranes are characterized by a large specific surface area, high porosity, and excellent mechanical properties. As a result, they are widely applied in multiple fields<sup>[12]</sup>. Sopan et al. investigated the application of electrospinning technology in the field of drug nanofibers. Their results indicated that electrospun nanofibers are a key carrier for enhancing drug efficacy and safety, with distinct advantages: strong loading capacity to improve drug storage stability; support for multi-component loading and precise controlled release of drugs; and the ability to enhance drug solubility and bioavailability, thereby reducing the required dosage and medication risks<sup>[13]</sup>. Li et al. investigated the antibacterial application of electrospinning. Focusing on electrospinning technology, they prepared nanofibers composed with antibacterial materials (synthetic organics, inorganic particles, etc.) and characterized their properties. The results confirmed that the antibacterial activity of nanofibers is structure-dependent, with diverse antibacterial mechanisms and significant advantages in multiple fields like wound dressings and water purification<sup>[14]</sup>. Notably, electrospun nanofiber membranes also exhibit remarkable adsorption capacities for dyes, particularly reactive dyes such as MB. For instance, Cen<sup>[15]</sup> et al. prepared a zinc-based metal-organic framework/titanium dioxide nanocomposite via electrospinning. This composite maintained a high photocatalytic degradation efficiency of 88.7 % even after five cycles. Zhang<sup>[16]</sup> et al. fabricated a cellulose acetate/chitosan/titanium dioxide fiber membrane via

electrospinning, which achieved efficiently removal of humic acid through the synergistic effects of adsorption and photocatalysis.

Hemp cellulose, as a typical biomass material derived from renewable agricultural resources, exhibits remarkable environmental value and sustainability advantages. It is biodegradable, low-cost, and abundant in nature, which aligns with the global pursuit of green and circular economy development. Compared with synthetic adsorbents, biomass-based materials like hemp cellulose not only reduce environmental pollution caused by non-degradable waste but also realize the high-value utilization of natural resources, making them promising candidates for environmental remediation applications<sup>[17,18]</sup>. Hemp cellulose inherently possesses a porous structure. Materials fabricated from cellulose offer advantages such as low density, high porosity, and a large specific surface area<sup>[19,20]</sup>. Polyacrylonitrile exhibits good mechanical and physical properties, a large specific surface area, and high chemical stability, thus being widely utilized in the textile industry<sup>[21,22]</sup>. By integrating the unique properties of hemp and polyacrylonitrile, a hemp/polyacrylonitrile composite fiber membrane can be fabricated via electrospinning, leveraging the membrane separation and adsorption mechanism. This endows the membrane with significant potential for application in the dye-adsorption field.

Currently, research on the dye adsorption performance of hemp/polyacrylonitrile (PAN) composite fiber membranes remains relatively

limited. In this study, a hemp/PAN composite fiber membrane was fabricated via electrospinning technology, using a hemp solution and PAN as raw materials. The effects of electrospinning process parameters on the structural and functional properties of the composite membranes were systematically investigated. Subsequently, the membrane was applied to the adsorption of dyes in simulated textile printing and dyeing wastewater containing MB, offering certain technical support for clean production.

## 2. Experimental

### 2.1 Materials

The hemp (10 g/5 m) was obtained from Tailai Xiangze Limited Company. All solution preparation were distilled water (18.2 MΩ cm) without further purification. The hemp solution and polyacrylonitrile (PAN, 150,000 molecular weight) come from the laboratory. Anhydrous lithium chloride (analytically pure AR) was purchased from Sinopharm Chemical Reagent Co., Ltd. N, N-Dimethylacetamide (AR) was purchased from Sinopharm Chemical Reagent Co., Ltd. Sodium hydroxide (AR) was purchased from Liaoning Quanrui Reagent Co., Ltd. Hydrogen peroxide (30 % mass fraction, AR) was purchased from Tianjin Kaitong Chemical Reagent Co., Ltd. Hydrochloric acid (AR) was purchased from Liaoning Quanrui Reagent Co., Ltd. Methylene blue (AR) was purchased from Tianjin Zhiyuan Chemical Reagent Co., Ltd.

### 2.2 Experimental Methods

#### 2.2.1 Activation of Hemp Fibers

To improve the dissolution efficiency of hemp fibers, activation pretreatment was conducted first: a certain amount of hemp fibers was added to a 100 mL conical flask containing DMAc and oscillated at 35 °C for 2 h (120 r/min) to enhance reagent penetration, followed by heating at 140 °C for 2 h in a water bath to break partial hydrogen bonds. After suction filtration, the samples were dried at 60 °C to constant weight.

#### 2.2.2 Dissolution of Hemp Fibers

Hemp fibers were dissolved using a LiCl/DMAc solvent system. Single-factor experiments were conducted to optimize the dissolution process, with the mass fraction of LiCl, solid-liquid ratio (hemp fibers to LiCl/DMAc), heating temperature, and heating time as the key variables. The optimized dissolution parameters were determined as follows: LiCl mass fraction of 12%, solid-liquid ratio of 1:180 (g:mL), heating temperature of 120 °C, and heating time of 3 h. After dissolution, the mixture was stirred continuously at room temperature to obtain a homogeneous hemp solution with a cellulose content of 89.95%.

In the LiCl/DMAc system, LiCl dissociates into Li and Cl ions, which disrupt the hydrogen bond network within hemp fibers, weaken the intermolecular forces between cellulose chains, and increase the polarity of the solvent system. This process facilitates the complete dissolution of hemp fibers, providing a homogeneous solution for subsequent blending with the PAN solution.

### 2.2.3 Preparation of Hemp/Polyacrylonitrile Nanofibers by Electrospinning

#### Method

A 15% (mass fraction) PAN solution was prepared by dissolving PAN in DMAc under magnetic stirring. The optimized hemp solution was then blended with the PAN solution at a specific ratio to form the electrospinning dope. Single-factor experiments were further conducted to optimize the electrospinning process, with the mass fraction of the hemp solution in the blend, receiving distance, applied voltage, and solution feed rate as the optimization variables.

### 2.2.4 Investigation on the Dye Adsorption of Hemp/Polyacrylonitrile Composite Fiber Membrane

A 50 mg sample of the prepared hemp/PAN composite fiber membrane was placed in a conical flask containing 150 mL of MB solution with a specific concentration (10 mg/L, 20 mg/L, 30 mg/L, 40 mg/L). The conical flask was then placed in a gas-bath constant temperature oscillator. Set the temperature at 20 °C, 30 °C, 40 °C, and sample at different time intervals within the range of 0 to 360 minutes to observe the adsorption effect of the nanofiber membrane on the dye. The mass of the fiber membrane is 50 mg. Observe the adsorption effect of the nanofiber membrane on the dye.

## 2.3 Characterization

### 2.3.1 Fourier transform infrared spectroscopy (FTIR)

To elucidate the chemical structures of the two fiber membranes, a

Spectrum One infrared spectrometer manufactured by PerkinElmer Inc. (USA) was used for their characterization. The variation trends of functional groups in the two membranes were explored through the analysis of infrared spectra. The testing conditions were set as follows: the wavenumber scanning range was  $4000 - 400 \text{ cm}^{-1}$ , the resolution was set at  $4 \text{ cm}^{-1}$ , and the number of scans was 30.

#### 2.3.2 X-ray diffraction (XRD)

The crystallization states of the two fiber membranes were characterized by a D8 X - ray diffractometer (Bruker, Germany). The testing conditions were as follows: the scanning rate was  $10 (\text{ }^\circ)/\text{min}$ , the voltage was set at 40 kV, the current was set at 200 mA, the  $2\theta$  range extended from  $3^\circ$  to  $90^\circ$ , and the scanning step size was  $0.01^\circ$ .

#### 2.3.3 X-ray photoelectron spectroscopy (XPS)

An ESCALAB250Xi X - ray photoelectron spectrometer (Thermo Fisher Scientific Inc., USA) was utilized to analyze and test the two fiber membranes. The purpose was to examine the chemical composition of the sample surfaces and analyze the differences in elemental content and distribution on the surfaces of the two nanofiber membranes.

#### 2.3.4 Scanning electron microscope (SEM)

The surface morphology of the fiber membrane was characterized with an S - 3400 scanning electron microscope (Hitachi, Japan). The testing conditions were as follows: the voltage was set at 10 kV, the ambient

temperature was maintained at  $15 \pm 5$  °C, and the ambient humidity was kept at  $50 \pm 3$  %.

### 2.3.5 Porosity

The porosity of the fiber membranes was characterized and calculated by the immersion method. First, the membrane was cut into a circle with a diameter of 0.9 cm. The area of the membrane was calculated. The thickness of the film was measured with a thickness gauge, and the membrane mass ( $M_1$ ) was recorded using an analytical balance. Then, the membrane was immersed in an n - butanol solution for 2 h and taken out. After using filter paper to blot the excess liquid on the surface of the fiber membrane, weight it and record the weight as  $M_2$ . The calculation formula for the porosity  $P$  is :

$$P = \frac{M_2 - M_1}{\rho_0 S T} \times 100\% \quad (1)$$

In the formula:  $S$ : The area of the membrane,  $\text{cm}^2$ ;  $\rho_0$ : The density of n-butanol, and its value is  $0.81 \text{ g/cm}^3$ ;  $T$ : The thickness of the membrane.

### 2.3.6 Particulate Matter Filtration Efficiency

The filtration efficiency of the prepared fiber membranes was tested with a particulate matter filtration efficiency tester. The gas temperature was set at  $20$  °C, and the gas flow rate was set at  $5 \text{ L/min}$ . The aerosol source was dry and stable compressed gas. The particulate matter counting efficiencies were  $50$  % for  $0.3 \mu\text{m}$  particles and  $98$  % for  $0.5 \mu\text{m}$  particles. The number concentration of particulate matter was in the range of  $65536/0.1 \text{ L}$ . The resistance test range was  $0 - 2000 \text{ Pa}$  with a resolution of  $0.1 \text{ Pa}$ , and the test

was carried out 20 times. The calculation formula for the filtration efficiency is as follows :

$$E = \frac{A_1 - A_2}{A_1} \times 100\% \quad (2)$$

In the formula: E: The filtration efficiency, A<sub>1</sub>: The number of particulate matters before filtration, A<sub>2</sub>: The number of particulate matters after filtration.

### 2.3.7 Mechanical and Physical Properties

The breaking tenacity and elongation at break of the nanofiber membrane were tested with an LLY - 06E electronic single - fiber strength tester (Laizhou Electronic Instrument Co., Ltd.). The testing conditions were as follows: the ambient temperature was set at 15 °C, the ambient humidity was set at 40 %, the linear density was 7.67 dTex, the gauge length was 20 mm, and the stretching rate was 30 mm/min. The nanofiber membrane had a length of 60 mm and a width of 15 mm. After all the samples were tested, the average values were calculated.

### 2.3.8 Water Drop Contact Angle

The contact angle of the hemp/PAN composite fiber membrane was measured with a fully - automatic JY - 82C video contact - angle measuring instrument (Chengde Dingsheng Testing Machine Inspection Equipment Co., Ltd.) to assess its hydrophilicity. The composite fiber membrane was cut into pieces measuring 40 mm in length and 20 mm in width. The testing environmental conditions were as follows: the ambient temperature was set

at 20 °C and the ambient humidity was set at 60 %.

### 2.3.9 Test of the standard curve of MB

The absorbance of pre - prepared MB solutions with different concentrations was measured using an ultraviolet - visible spectrophotometer. The maximum absorption wavelength of MB was determined to be 664 nm. The concentration and absorbance were designated as X and Y respectively, the standard curve of MB is  $y = 0.1098x + 0.566$ , with a correlation coefficient of  $R^2 = 0.9714$ .

### 2.3.10 Adsorption Rate of the Fiber Membrane

An ultraviolet spectrophotometer was used to measure the mass concentration of the MB solution before and after the fiber membrane's adsorption. The removal efficiency of the fiber membrane was calculated according to the following formula<sup>[23]</sup>:

$$P = \frac{C_0 - C_e}{C_0} \times 100\% \quad (3)$$

In the formula, P: The removal efficiency, %;  $C_0$ : The initial mass concentration of the dye, mg/L;  $C_e$ : The mass concentration at equilibrium after adsorption, mg/L.

### 2.3.11 Adsorption Kinetics

MB solutions with mass concentrations of 15 mg/L, 30 mg/L, and 45 mg/L were respectively prepared. A 50 mg fiber membrane was added to each solution. At different time intervals within the range of 0 to 360 minutes, a certain volume of the solution was sampled. After centrifugation, the

supernatant was taken. The mass concentration of the MB solution in the supernatant was measured using a JC - T6000 IoT intelligent ultraviolet - visible spectrophotometer (Qingdao Juchuang Environmental Protection Group Co., Ltd.). The adsorption capacity of the fiber membrane was calculated according to the following formula<sup>[24]</sup>:

$$q = \frac{(C_0 - C_t)V}{m} \quad (4)$$

In the formula,  $C_0$ : The initial mass concentration, mg/L;  $C_t$ : The mass concentration at the time interval  $t$ , mg/L;  $V$ : The total volume of the solution, L;  $m$ : The mass of the adsorbent, g.

The formula of the pseudo-first-order kinetic model<sup>[25]</sup>:

$$\ln(q_e - q_t) = \ln q_e - k_1 t \quad (5)$$

The formula of the pseudo-second-order kinetic model :

$$\frac{t}{q_t} = \frac{1}{k_2 q_e^2} + \frac{t}{q_e} \quad (6)$$

The formula of the internal diffusion model :

$$q_t = Kt^{\frac{1}{2}} + c \quad (7)$$

In the formula,  $k_1$ : The pseudo - first - order kinetic constant,  $\text{min}^{-1}$ ;  $k_2$ : The pseudo - second - order kinetic constant,  $\text{g}/(\text{mg}\cdot\text{min})$ ;  $q_e$ : The adsorption capacity of the fiber membrane at adsorption equilibrium,  $\text{mg}/\text{g}$ ;  $q_t$ : The adsorption capacity of the fiber membrane at time  $t$ ,  $\text{mg}/\text{g}$ ;  $K$ : The diffusion rate constant,  $\text{g}/(\text{mg}\cdot\text{min}^{0.5})$ ;  $c$ : The boundary layer thickness.

### 2.3.12 Adsorption Isotherm

The temperature of the water - bath constant - temperature shaker was

set at 20 °C, 30 °C, and 40 °C, while the shaking speed was set at 200 r/min. For each temperature setting, 150 mL of MB solutions with different mass concentrations were taken, and a 50 mg fiber membrane was added to each solution for shaking adsorption. After the adsorption equilibrium was reached, the solution was centrifuged. The supernatant was then taken and its absorbance was measured. The obtained isotherm data were fitted with the Langmuir model and the Freundlich model. The formula of the Langmuir model<sup>[26]</sup> :

$$\frac{C_e}{q_e} = \frac{C_e}{q_m} + \frac{1}{q_m b} \quad (8)$$

The formula of the Freundlich model<sup>[27]</sup>:

$$\log_2 q_e = \log_2 K_F + \frac{1}{n} \log_2 C_e \quad (9)$$

In the formula:  $q_m$ : The maximum adsorption capacity, mg/g.  $b$ : The equilibrium constant of the Langmuir model, L/mg.  $C_e$ : The mass concentration of MB at adsorption equilibrium, mg/L.  $K_F$ : The adsorption equilibrium constant of the Freundlich model,  $(\text{mg/g})/(\text{mg/L})^{\frac{1}{n}}$ .  $n$ : The adsorption intensity constant of the Freundlich model.

### 3. Results and Discussion

#### 3.1 Study on the Influencing Factors of the Electrospinning Process of Hemp/Polyacrylonitrile Composite Fiber Membranes

In the investigation of the electrospinning process of hemp/PAN composite fiber membranes, key factors significantly influencing the

electrospinning process were comprehensively discussed. These factors included the mass fraction of the cellulose solution (8 %, 10 %, 12 %, 14 %), the receiving distance (10 cm, 15 cm, 20 cm, 25 cm), the voltage (18 kV, 20 kV, 22 kV, 24 kV), and the liquid - pushing speed (0.5 mL/h, 1 mL/h, 1.5 mL/h, 2 mL/h). By employing a scanning electron microscope and taking the fiber diameter as well as the mechanical and physical properties as evaluation indexes, the experimental results are presented in **Fig. 1**.

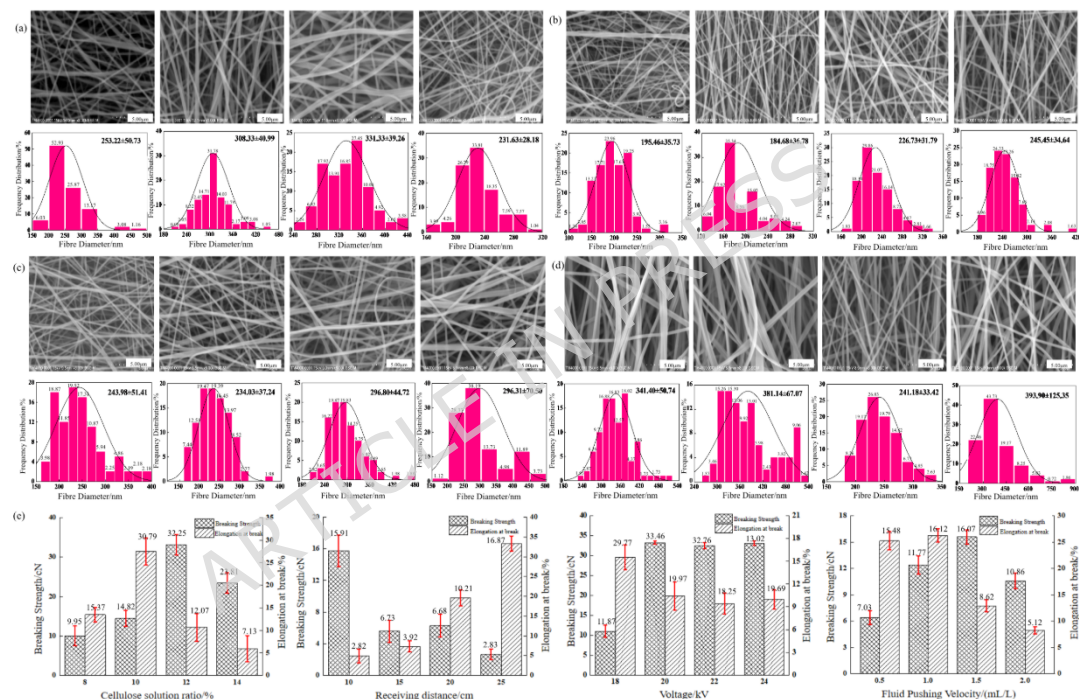


**Fig. 1.** (a), (b), (c) and (d) are the scanning electron microscopy images and fiber diameter diagrams of cellulose solutions with different mass fractions, receiving distances, voltages and pushing liquid speeds respectively. (e) Mechanical physical property diagrams for cellulose solutions with different mass fractions, receiving distances, voltages, and syringe pump speeds.

As depicted in **Fig. 1** (a) (b) (c) and (d), when the mass fraction of the cellulose solution is 10 %, the fiber diameter predominantly ranges from 250

to 350 nm. The fiber diameter exhibits a uniform distribution, the surface of the fiber membrane is smooth, and the differences among the fibers are diminished. In contrast, when the mass fraction assumes other values, the gaps between fibers are non-uniform. The surface appears rough rather than smooth, with beads forming and bending phenomena occurring. When the receiving distance is 20 cm, the fiber diameter mainly spans from 180 to 260 nm. The distribution of the fiber diameter is relatively concentrated, the fiber surface is smooth, and there are no occurrences of knotting or bending. Overall, the electrospinning effect is favorable. Conversely, when the receiving distance takes on other values, the fiber surface is not smooth, and bending phenomena arise. The gaps between the fibers are larger compared to when the receiving distance is 20 cm, and the distribution range of the fiber diameter is relatively broad. The study revealed that as the receiving distance varies while the voltage remains constant, the intensity of the electric field gradually declines, which in turn causes a change in the frequency - distribution state of the fiber diameter. Selecting a receiving distance that is either too short or too long may result in the formation of beaded fibers. When the voltage is 20 kV, the fiber diameter is concentrated within the range of 160 - 300 nm. The fiber distribution is relatively concentrated, and the surface uniformity is good. When the voltage assumes other values, the distribution of the fiber diameter is relatively dispersed and cannot be concentrated within a narrow range. At this point, the gaps

between the fibers are relatively large, and the diameters are generally larger than those in the previous case. When the liquid - pushing speed is 1.5 mL/h, the fiber diameter mainly ranges from 200 to 280 nm. The fiber diameter is smaller than that at the previous two liquid - pushing speeds, and the uniformity is good. When the liquid - pushing speed takes on other values, the distribution range of the fiber diameter is relatively wide, the gaps between the fibers are large, the uniformity is mediocre, and the electrospinning effect is poor. The hydroxyl groups in the hemp cellulose form hydrogen bonds with the functional groups in the polymer. This interaction contributes to the good orientation of the fibers in the membrane, resulting in uniform fiber arrangement and no obvious aggregation. In addition, there is good compatibility between hemp fibers and PAN. This compatibility ensures that during the electrospinning process, the composite solution can be spun into fibers with a more consistent diameter and fewer defects. If the compatibility is poor, as seen when the mass fraction of the hemp solution is too high, the film-forming property is poor, and the mechanical and physical properties are also affected. The SEM images clearly show that when the compatibility is good, the surface of the fiber membrane is smooth, while poor compatibility leads to a rough surface with uneven fiber distribution. **Fig. 1** (e) further confirms, which presents the mechanical and physical test results, the thickness of the fiber membrane during the test was measured as  $0.094 \pm 0.003$ . By selecting a cellulose -

solution mass fraction of 10 %, an optimal receiving distance of 20 cm, a voltage of 20 kV, and a liquid - pushing speed of 1.5 mL/h for blending with the PAN solution, a better electrospinning effect can be achieved.

### 3.2 Testing and Analysis of Hemp/Polyacrylonitrile Nanofiber Membranes

To clarify the structure-performance relationship of hemp/PAN composite membranes, multi-dimensional characterization (contact angle, FTIR, XRD, XPS) and functional tests (porosity, filtration efficiency) were carried out, with results discussed as follows.

#### 3.2.1 Characterization and Analysis of Water Drop Contact Angle, Structure, and Composition of Hemp/Polyacrylonitrile Composite Fiber Membrane

If the water drop contact angle is greater than 90°, it indicates that the material is hydrophobic; if the water drop contact angle is less than 90°, it indicates that the material is hydrophilic<sup>[28]</sup>. The water drop contact angle test results of the hemp/PAN composite fiber membrane are shown in **Fig. 2**

(a). Considering that PAN is hydrophobic and hemp is hydrophilic, a water drop contact - angle tester was used to drip a drop of water onto the surface of the hemp/PAN composite fiber membrane. The shape of the water drop was observed 1 second after dripping, and the corresponding contact angle was measured. The first image depicts the morphology of the water droplet before it lands on the membrane surface; the second image shows the state of the water droplet on the membrane surface one second later, at which

time the water droplet has partially infiltrated the membrane surface; the third image represents the state after a certain period of time (before the water droplet is completely absorbed). The hemp fibers contain numerous hydrophilic hydroxyl groups, and their hydrophilicity is retained in the composite membrane. The average water contact angle was  $14.51^\circ$ , indicating good hydrophilicity. Due to the nanopores, the water drop was completely absorbed within 2 s.

The characterizations of Fourier transform infrared spectroscopy (FTIR), X-ray diffraction (XRD) and X-ray photoelectron spectroscopy (XPS) for the PAN fiber membrane and the hemp/PAN composite fiber membrane are shown in **Fig. 2** (b) (c) (d). The hydroxyl groups in the cellulose of hemp fibers can form hydrogen bonds with the functional groups in the PAN polymer. This hydrogen bonding interaction promotes the uniform dispersion of hemp cellulose in the PAN matrix. Analyze the changes of various characteristic absorption peaks, crystalline regions and the contents of surface fiber elements. In the infrared spectrum of the hemp/PAN composite fiber membrane. The peak formed at  $3401\text{ cm}^{-1}$  is the characteristic absorption peak of the -OH stretching vibration in the cellulose component<sup>[29]</sup>. The peak appearing at  $2929\text{ cm}^{-1}$  belongs to the characteristic absorption peak of the C-H stretching vibration of lignin<sup>[30]</sup>. The peak formed at  $1731\text{ cm}^{-1}$  is attributed to the characteristic absorption peak of the C=O stretching vibration of the carboxylic acid and its esters in

xylan. The peaks at 1452, 1359, 1142, 1066 and 1029  $\text{cm}^{-1}$  are related to the characteristic absorption peaks of cellulose<sup>[31-33]</sup>. These spectral characteristics confirm the existence of strong interactions between hemp and PAN. And the composite membrane retains the structural properties of the natural polymers in hemp fibers. The absorption peaks in the infrared fingerprint region (1300 - 400  $\text{cm}^{-1}$ ) of the composite membrane show a high degree of similarity to the standard spectrogram of hemp fibers, indicating that the composite process with PAN has not significantly changed the chemical structural framework of the original cellulose. The van der Waals forces between the hemp cellulose and PAN polymer also influence the morphology. By comparing the spectral characteristics of the composite membrane with those of PAN and hemp fibers, the chemical adsorption mechanism can be indirectly verified. The peak at 3401  $\text{cm}^{-1}$  in the composite membrane is broader and weaker than that in pure hemp fibers, indicating that hydroxyl groups are involved in interactions with MB (such as hydrogen bonding or complexation). Additionally, the characteristic peak of the cyano group (-CN) stretching vibration at 2243  $\text{cm}^{-1}$  in PAN slightly shifts to a lower wavenumber (2238  $\text{cm}^{-1}$ ) in the composite membrane, which may be attributed to the interaction between the nitrogen-containing groups in PAN and MB molecules. These spectral changes, combined with the fitting results of the pseudo-second-order kinetic model and the Langmuir adsorption isotherm model, collectively confirm that the

adsorption process is dominated by chemical adsorption. The XRD spectrum of the hemp/PAN composite fiber membrane shows characteristic diffraction peaks at  $2\theta=21^\circ\sim24^\circ$ , corresponding to the (002) crystal plane of cellulose I structure, while retaining some PAN diffraction peaks. Compared with pure PAN membranes, the composite membrane's crystal structure changes due to van der Waals forces between hemp cellulose and PAN, evidenced by similar diffraction peaks at  $2\theta=3^\circ\sim20^\circ$ <sup>[34-37]</sup>. XPS analysis shows binding energies at 285.08 eV (C1s), 398.08 eV (N1s), and 531.08 eV (O1s), with stronger peak intensities in the composite membrane, indicating increased contents of C, O, and N elements after hemp-PAN blending.

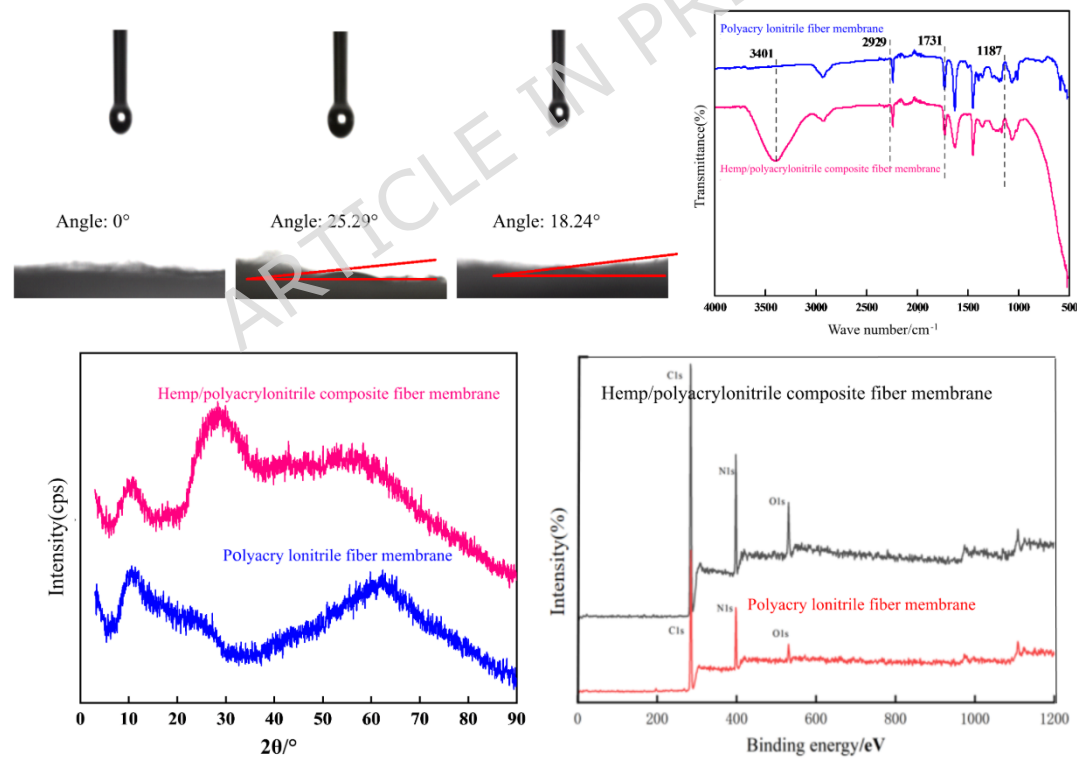


**Fig. 2.** (a) Effect Diagram of the Water Drop Contact Angle of the Nanofiber Membrane. (b) FTIR of PAN and Hemp/PAN Composite Fiber Membrane. (c) XRD Patterns of PAN Fiber Membrane and Hemp/PAN

Composite Fiber Membrane. (d) XPS Patterns of PAN Fiber Membrane and Hemp/PAN Composite Fiber Membrane.

The differences in C1s, O1s, and N1s contents shown in **Fig. 3** provide direct evidence for the interfacial compatibility of hemp/PAN composite membranes: the surface C and N contents of pure PAN membranes are 77.7% and 15.7% respectively, while those in composite membranes increase to 77.83% and 16.63%, and O element also shows a characteristic signal due to the introduction of hemp cellulose. This change stems from two aspects: first, hemp cellulose takes C as the core element (C accounts for more than 44% in the molecule), and its uniform dispersion slightly increases the C content on the membrane surface; second, the hydroxyl groups of cellulose form hydrogen bonds with the cyano groups (-CN) of PAN. This strong interaction promotes the oriented arrangement of PAN molecular chains on the surface of hemp components, reducing the burial probability of N elements and leading to a significant increase in surface N content. The synergistic change of element contents breaks the limitation of "easy delamination in physical blending", confirming that there is a stable interfacial bonding between hemp and PAN matrix rather than simple mechanical mixing, which also lays a structural foundation for the improvement of subsequent adsorption performance and mechanical stability of the composite membrane.

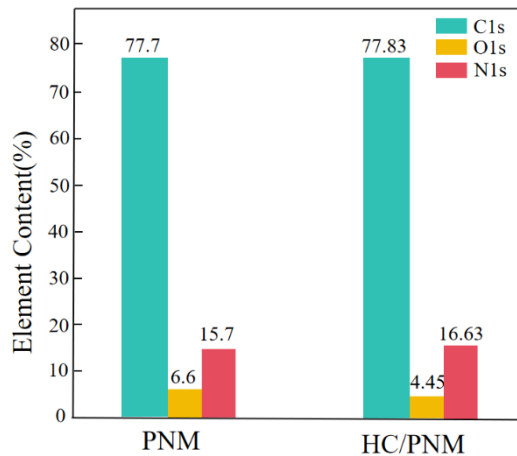


**Fig. 3.** Proportions of the Contents of Three Elements, C1s, O1s and N1s, in the Two Kinds of Fiber Membranes.

### 3.2.2 Porosity Analysis

The porosities and thicknesses of the two kinds of fiber membranes are shown in **Fig. 4**. Data in **Fig. 4** show that the porosity of the hemp/PAN composite fiber membrane is slightly higher than that of the pure PAN fiber membrane. This phenomenon is not only attributed to the natural porous structure of hemp cellulose, but also closely related to the "phase separation effect" during the blended spinning process — the branched hydroxyl groups on hemp cellulose molecular chains form local hydrogen bonding with the cyano groups of PAN molecular chains. This heterogeneous interfacial interaction breaks the tight packing mode of PAN molecular chains, leading to the formation of micro-pores at the two-phase interface when the spinning solution solidifies into a membrane. Combined with the inherent porous characteristics of hemp cellulose, a more abundant hierarchical pore structure is co-constructed; the high porosity provides a "fast channel" for

the mass transfer of MB dye molecules, which not only reduces the diffusion resistance of molecules in the membrane, but also fully utilizes the adsorption sites (such as hydroxyl and cyano groups) on the membrane surface and inside, avoiding the problem of "surface adsorption saturation and internal site idleness" in pure PAN membranes due to low porosity. Ultimately, the adsorption performance is improved through the synergistic effect of "structure-mass transfer-adsorption" [38].

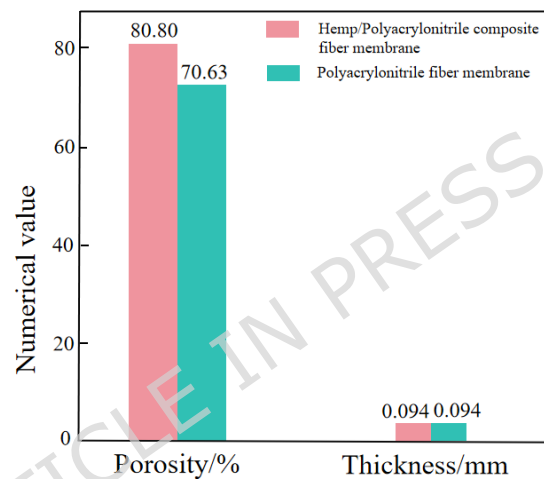


**Fig. 4.** Porosities and Thicknesses of the Two Kinds of Fiber Membranes.

### 3.2.3 Particle Filtration Efficiency Analysis

The particle concentrations and numbers of the fiber membranes are shown in **Table 1**.

**Table 1.** The test data of the particles in the fiber membrane.

No	PM1.0		PM2.5		PM10		Number of Particles			
	Concentration $\mu\text{g}/\text{m}^3$						0.3 $\mu\text{m}$		0.5 $\mu\text{m}$	
	Before	After	Before	After	Before	After	Before	After	Before	After
	Filtration	Filtration	Filtration	Filtration	Filtration	Filtration	Filtration	Filtration	Filtration	Filtration
1	9	0	9	0	9	0	3552	0	963	0
2	10	0	10	0	10	0	3819	0	1033	0
3	15	0	15	0	15	0	5883	0	1605	0

4	17	0	17	0	17	0	6708	0	1860	0
5	22	0	22	0	22	0	8553	0	2370	0
6	39	0	39	0	39	0	15144	0	4282	0
7	61	0	61	0	61	0	23157	4	6605	3
8	71	0	71	0	71	0	27030	7	7688	5
9	80	0	80	0	80	0	30786	9	8711	6
10	86	0	86	0	86	0	33561	6	9433	4
11	87	0	87	0	87	0	34119	5	9597	2
12	79	0	79	0	79	0	32070	10	8856	2
13	74	0	74	0	74	0	30408	6	8344	2
14	67	0	67	0	67	0	28605	9	7776	3
15	59	0	59	0	59	0	25431	5	6879	1
16	54	0	54	0	54	0	23535	5	6373	3
17	53	0	53	0	53	0	23034	3	6231	2
18	52	0	52	0	52	0	22923	3	6183	1
19	51	0	51	0	51	0	22530	4	6078	2
20	49	0	49	0	49	0	21444	2	5788	1
Average Value	51.75	0	51.7	0	51.7	0	21114	3.9	5832	1.8
Filtration										
n							99.97 %			
Efficiency										
cy										

Upon observing **Table 1**, it can be noted that the data prior to filtration are relatively large, whereas those after filtration are relatively small. This indicates that the fiber membrane prepared in this study demonstrates excellent filtration performance when used to filter particulate matter in the air. Through calculation, the filtration efficiency is found to reach 99.97 %. It is noteworthy that the high porosity of the composite fiber membrane is the core linking factor for its excellent particulate matter filtration efficiency and dye adsorption performance. From the perspective of functional synergistic mechanism: on one hand, the high porosity and uniform fiber diameter distribution provide sufficient retention space for air particles, achieving 99.97% high-efficiency filtration through mechanisms such as interception

and inertial impaction; on the other hand, the well-developed porous structure not only increases the specific surface area of the membrane but also provides more diffusion channels and adsorption active sites (e.g., cellulose hydroxyl groups, PAN nitrogen-containing groups) for MB dye molecules, promoting the rapid penetration of dye molecules into the membrane and chemical adsorption. This "porous structure-dual function synergy" characteristic endows the composite membrane with unique multifunctional advantages in complex application scenarios (such as integrated waste gas purification and wastewater treatment in printing and dyeing workshops), expanding its practical application scope.

The high porosity of the composite membrane is the core structural basis for achieving the synergy of high-efficiency filtration and high-efficiency adsorption: On one hand, the uniformly distributed nano-scale pores and fiber diameters provide sufficient retention space for air particles, achieving a filtration efficiency of 99.97% through mechanisms such as interception and inertial impaction; On the other hand, this hierarchical pore structure also provides rapid diffusion channels for MB dye molecules, reducing the mass transfer resistance of molecules in the membrane, so that the adsorption active sites on the membrane surface and inside can be fully utilized, avoiding the problem of 'surface adsorption saturation and internal site idleness' in pure PAN membranes due to low porosity. In addition, the good hydrophilicity of the composite membrane not only accelerates the

penetration of dye solution in the membrane, but also improves the wettability and stability of the membrane during filtration, further enhancing the synergy of the two functions.

### 3.3 Study on the Influences of Relevant Factors on the Adsorption of Dyes by the Hemp/Polyacrylonitrile Composite Cellulose Membrane

In the study of the adsorption of dyes by the hemp/PAN composite fiber membrane, the key factors such as the mass fraction of the hemp solution (8 %, 10 %, 12 %, 14 %), the heating temperature (20 °C, 30 °C, 40 °C, 50 °C), the concentration of MB (10 mg/L, 20 mg/L, 30 mg/L, 40 mg/L), the pH value (3, 5, 7, 9), and the heating time (5 h, 7 h, 9 h, 11 h) were deeply explored for their influences on the adsorption rate of the composite cellulose membrane. Taking the adsorption rate of MB dye as the evaluation index, the experimental results are shown in **Fig. 5**.

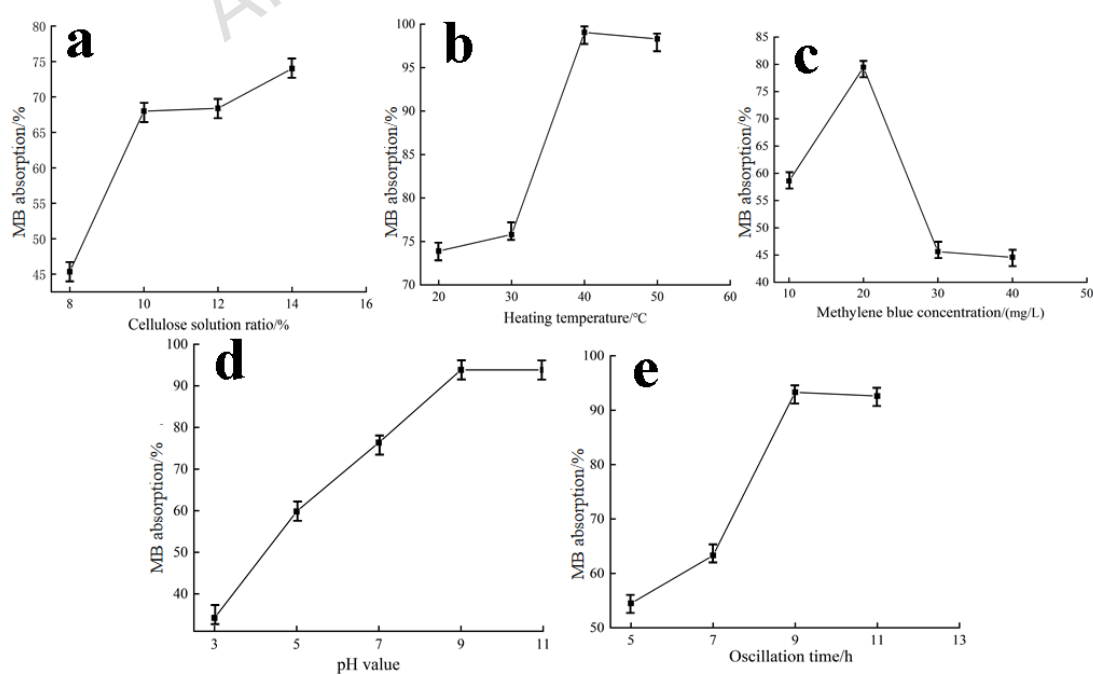


**Fig. 5.** Influence of Different Factors on the Dye Adsorption of the Fiber Membrane.

**Fig. 5** reveals the regulatory mechanisms of key parameters on MB adsorption by composite membranes via the single-factor method, thereby determining the optimal conditions: Cellulose proportion (**Fig. 5a**) requires balancing adsorption sites and membrane performance — 10% is optimal (14% causes 32% lower membrane strength due to agglomeration, and the adsorption difference between 10% and 12% is <2%); Temperature (**Fig. 5b**) peaks at 40 °C: heating accelerates MB diffusion to enhance adsorption before 40 °C, while exceeding 40 °C destroys hydrogen bonds and triggers desorption; MB concentration (**Fig. 5c**) is optimal at 20 mg/L (10 mg/L leaves sites idle, >30 mg/L saturates sites); pH=9 (**Fig. 5d**) strengthens membrane surface negativity (Zeta potential 18 mV lower than pH=7) to improve adsorption via electrostatic attraction; Heating time (**Fig. 5e**) reaches equilibrium at 9 h, and prolonged heating oxidizes hydroxyl groups to reduce activity. In conclusion, the optimal combination (10% cellulose, 40 °C, 20 mg/L MB, pH=9, 9 h) lays a foundation for subsequent optimization.

### 3.4 Experimental Results and Discussion of the Response Surface Methodology

Based on the results of the single - factor experiments, the optimal experimental ranges of the significant factors were selected. Then, response surface analysis was conducted with the adsorption rate of the dye as the

optimization objective. The experimental design table for the Box Behnken design is presented in **Table 2**, and the experimental results of the response surface are shown in **Table 3**.

**Table 2.** Box-Behnken Experimental Design with Three Factors and Three

Levels.

Level	Heating Temperature (°C)	Methylene blue concentration (mg/L)	Oscillation Time (h)
1	35	15	6
2	40	20	8
3	45	25	10

**Table 3.** Experimental Results of the Box-Behnken Response Surface

Methodology.

Experimental Number	Heating Temperature (°C)	Methylene blue concentration (mg/L)	Oscillation Time (h)	Adsorption Rate (%)
1	45	25	8	53.27
2	35	20	9	73.4
3	35	25	8	55.24
4	45	20	9	95.05
5	35	15	8	52.44
6	40	25	9	50.68
7	40	20	8	83.6
8	40	20	8	86.1
9	40	15	9	54.2
10	40	20	8	86.95
11	45	20	7	77.95
12	40	20	8	79.65
13	40	25	7	38.27
14	35	20	7	73.4
15	45	15	8	83.8
16	40	20	8	90.31
17	40	15	7	69.07

### 3.5 Analysis of Variance of the Quadratic Regression Model

To accurately quantify the influence of heating temperature (A), MB concentration (B), and shaking time (C) on the adsorption rate of hemp/PAN composite membranes and optimize the process parameters, this study established a quadratic regression model of adsorption rate based on Box-Behnken design, whose statistical characteristics and practical application value can be deeply interpreted through the data in Table 4: the coefficient of determination  $R^2$  of the model is 0.9742, meaning the model can explain 97.42% of the adsorption rate variation, which is much higher than the fitting requirement of general regression models (usually  $R^2 \geq 0.95$  is considered excellent fitting); the synergistic results of extremely significant model P-value  $<0.0001$  and non-significant lack-of-fit term  $P=0.4314>0.05$  not only confirm that the model equation has extremely high statistical reliability within the experimental range, but also indicate that the model does not miss key influencing factors, which can effectively avoid the interference of experimental errors on parameter optimization<sup>[39,40]</sup>; from the perspective of factor significance ranking reflected by F-value (B>A>C, i.e., MB concentration > heating temperature > shaking time), MB concentration, as the most critical influencing factor, has a much stronger regulatory effect on adsorption rate than shaking time, and this law is highly consistent with the essence of adsorption kinetics — MB concentration directly determines the saturation degree of adsorption sites on the membrane surface: when the concentration is low, sufficient sites lead to an increase in adsorption rate

with concentration; when the concentration is high, site saturation reduces the adsorption rate, while shaking time only indirectly affects the adsorption process by influencing mass transfer rate, so its regulatory priority is lower. This conclusion provides a clear direction for process optimization: the initial MB concentration should be prioritized to be controlled at around 20 mg/L (the optimal value of single-factor experiment), and then the heating temperature should be adjusted to 45°C and shaking time to 9 h in coordination, so as to achieve the maximum adsorption rate of 95.05%. This model-based precise regulation scheme is more scientific and operable than traditional single-factor optimization, avoiding cost waste caused by blind experiments.

**Table 4.** Establishment of the Response Surface Regression Model and Significance Analysis.

Project	Sum of Squares	Freedom	Mean Square	Variance Ratio	P Value	Significance
Model	4449.69	9	494.41	29.379	<0.0001	Yes
A	386.28	1	386.28	22.954	0.0020	
B	481.28	1	481.28	28.599	0.0011	
C	26.79	1	26.79	1.5920	0.2475	
AB	277.72	1	277.72	16.503	0.0048	
AC	73.10	1	73.10	4.3440	0.0756	
BC	186.05	1	186.05	11.055	0.0127	
$A^2$	8.02	1	8.02	0.4767	0.5122	
$B^2$	2741.06	1	2741.06	162.88	<0.0001	
$C^2$	191.97	1	191.97	11.407	0.0118	

Residual	117.80	7	16.83			
Misfitting Term	54.52	3	18.17	1.1490	0.4314	No
Pure Error	63.27	4	15.82			
Total						
Deviation	4567.49	16				
n						
R <sup>2</sup>	0.9742					
R <sup>2</sup> <sub>Adj</sub>	0.9411					

In order to further confirm that the fitting regression equation of the response surface design experiment is of significant significance, a multiple regression was carried out, and the obtained quadratic regression equation is :

$$\begin{aligned}
 Y = & -3.20105A + 41.69235B + 48.386C - 0.3333AB + 0.855AC \\
 (10) \quad & + 1.364BC + 0.05521A^2 - 1.02059B^2 - 6.75225C^2 - 480.727
 \end{aligned}$$

Response-surface and contour plots based on the regression equation showed the effects of heating temperature, MB concentration, and shaking time on the nanofiber membrane's adsorption rate. The optimal conditions were determined as: heating temperature 45 °C, MB concentration 20 mg/L, shaking time 9 h, yielding a maximum adsorption rate of 95.05 %. Substituting into the regression model gave a predicted value of 93 %, with a 2 % deviation. With R<sup>2</sup>=0.9742, the model results were within the error range, indicating good fitting between predicted and experimental values.

**Fig. 6** (a) shows the interactive effect of heating temperature and MB concentration on dye adsorption rate. With constant shaking time, the

adsorption rate first increases then decreases as both factors rise. **Fig. 6** (b) depicts the interaction between heating temperature and shaking time: at fixed MB concentration, adsorption rate gradually increases with both factors, though the significance index  $P > 0.05$  indicates no significant effect. **Fig. 6** (c) illustrates the interaction of MB concentration and shaking time: at fixed heating temperature, adsorption rate first increases then decreases as both factors rise.

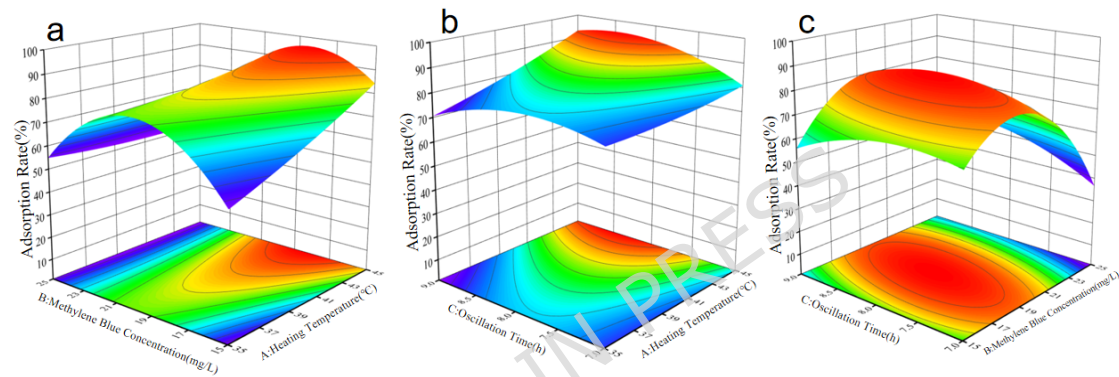


**Fig. 6.** (a) (b) and (c) are the response surface plots of the influences of the interactions between the heating temperature and the concentration of MB, between the heating temperature and the shaking time, and between the concentration of MB and the shaking time on the adsorption rate of the dye, respectively.

### 3.6 Analysis of adsorption kinetics and adsorption isotherms for hemp/polyacrylonitrile composite fiber membranes

**Fig. 7** (a) (b) (c) shows the adsorption kinetics model of the hemp/PAN composite fiber membrane. As shown in **Table 5**, the pseudo-second-order kinetics model has a better fitting performance with  $R^2$  closer to 1, signifying a higher linear correlation between the dependent and independent

variables<sup>[41]</sup>. The adsorption of MB by the membrane follows the pseudo-second-order model, suggesting dominant chemical adsorption. The -OH groups in hemp cellulose and nitrogen-containing groups in PAN form chemical bonds or strong interactions with MB, leading to the slow adsorption process described by this model. Based on the material composition and adsorption characteristics, the types of chemical interactions are inferred as follows: (1) Hydrogen bonding: The hydroxyl groups (-OH) in hemp cellulose form hydrogen bonds with the lone-pair electrons on the nitrogen atoms of MB; the amino groups (-NH<sub>2</sub>) generated by the hydrolysis of cyano groups (-CN) in PAN can also bond with the aromatic rings of MB, enhancing the adsorption force. (2) Electrostatic attraction: Under the alkaline condition of pH=9, cationic MB carries a positive charge, the carboxyl groups (-COOH) in hemp cellulose dissociate to carry a negative charge, and the weakened protonation of amino groups in PAN renders the membrane surface weakly negatively charged, enabling rapid adsorption through electrostatic attraction. (3) Complexation: The hydroxyl groups in hemp cellulose and the nitrogen atoms in PAN act as coordination atoms, forming weak complexes with the metal ions (if present) or aromatic rings of MB to stabilize the adsorption system. These multiple interactions collectively dominate the adsorption process, which is consistent with the fitting result of the pseudo-second-order kinetic model (controlled by chemical adsorption). The electrospun membrane's large specific surface

area and high porosity enable rapid initial physical adsorption via van der Waals forces, while chemical adsorption becomes the rate-determining step as sites saturate. **Fig. 7 (c)** and **Table 6** show the adsorption process involves three diffusion stages (surface > mesopore > micropore) with  $K_1 > K_2 > K_3$ , meaning surface diffusion > mesopore diffusion > micropore diffusion, which indicates that the adsorption rate of the fiber membrane is governed by internal diffusion<sup>[42,43]</sup>.

The adsorption isotherm reflects the equilibrium relationship between adsorbent capacity and adsorbate concentration at a given temperature, aiding in understanding adsorption mechanisms and determining maximum adsorption capacity, which is crucial for evaluating adsorbent performance in practical applications like printing and dyeing wastewater treatment<sup>[44-47]</sup>.

**Table 7** and **Fig. 7 (d) (e) (f)** show the adsorption isotherm parameters and models of the hemp/PAN composite fiber membrane. As shown in **Fig. 7 (d)**, the adsorption capacity for MB increases with temperature, reaching 76.97 mg/g at 40°C<sup>[48]</sup>. The Langmuir model fits better (higher  $R^2$  in **Table 7**), indicating the membrane has a uniform surface and undergoes monolayer adsorption.

The adsorption thermodynamics analysis is used to determine whether the entire adsorption reaction is a spontaneous reaction. The formulas are as follows<sup>[49]</sup>:

$$\Delta G = \Delta H - T\Delta S$$

(11)

$$\ln \frac{q_e}{C_e} = \frac{\Delta S}{R_0} - \frac{\Delta H}{R_0 T}$$

(12)

$$\Delta G = -R_0 \ln \frac{q_e}{C_e}$$

(13)

$$\Delta G^0 = -RT \ln K$$

(14)

In the formulas,  $\Delta G$ : The Gibbs free energy, kJ/mol.  $\Delta S$ : The entropy change, J/(mol·K).  $\Delta H$ : The enthalpy change, kJ/mol.  $R_0$ : The gas constant, taking the value of 8.314 J/(mol·K).  $T$ : The absolute temperature, K.  $K$ : Adsorption equilibrium constant.

The acquisition and analysis of adsorption thermodynamic parameters all focus on the intrinsic mechanism of MB adsorption by hemp/PAN composite membranes: As intrinsic energy characteristics of the adsorption process,  $\Delta S$  (entropy change) and  $\Delta H$  (enthalpy change) were calculated from the linear fitting of  $\ln(q_e/C_e)$  versus  $1/T$  in **Fig. 7 (g)** (the slope corresponds to  $\Delta H/R$  and the intercept corresponds to  $\Delta S/R$ , where  $R$  is the gas constant), and a complete parameter matrix was further derived by combining adsorption isotherm data at different temperatures (**Table 8**); this calculation method based on the quantitative correlation between thermodynamics and adsorption equilibrium ensures parameter reliability<sup>[50,51]</sup>;  $\Delta G$  was negative under all temperature conditions and its absolute value increased with temperature ( $\Delta G = -1.4491$  kJ/mol at 20°C and increased to -3.0223 kJ/mol at 40°C), which not only confirms that the adsorption is a spontaneous process but also reveals that high temperature

can enhance the spontaneity of adsorption by accelerating MB molecule diffusion, reducing liquid film resistance, and strengthening the specific interaction between molecules and hydroxyl/nitrogen-containing groups on the membrane surface, providing direct basis for optimizing the adsorption temperature to approximately 40°C to achieve high efficiency and low consumption; the synergistic characteristics of positive  $\Delta S$  (87.5441 J/(mol·K)) and positive  $\Delta H$  (24.1223 kJ/mol) clarify the energy and entropy change mechanism of adsorption — positive  $\Delta S$  arises from the disruption of water molecule binding during MB molecule immobilization and the molecular dispersion effect brought by the membrane's porous structure (porosity increased by 8.2% compared with pure PAN membrane), significantly increasing the system disorder; positive  $\Delta H$  confirms that the adsorption is an endothermic process, whose energy consumption can be compensated by increasing temperature, and the entropy-driven effect of  $\Delta S > 0$  dominates to ensure spontaneous adsorption<sup>[52]</sup>; this "endothermic adsorption driven by entropy increase" is essentially a reflection of the specific hydrogen bonding between hydroxyl groups of hemp cellulose and MB molecules — hydrogen bonds reduce the energy barrier, while entropy increase caused by molecular dispersion becomes the core driving force for spontaneous adsorption.

To clarify the performance level of the hemp/polyacrylonitrile (PAN) composite membrane prepared in this study among similar adsorbent materials, it was compared with representative adsorbents reported in the

literature. The maximum adsorption capacity of the material in this study (76.09 mg/g at 40°C) is 4% higher than that of the La(OH)<sub>3</sub>/PAN membrane (73.05 mg/g)<sup>[53]</sup> and significantly higher than another reported La(OH)<sub>3</sub>/PAN membrane (5.02 mg/g)<sup>[54]</sup>. In addition, this material exhibits an excellent particulate matter filtration efficiency of 99.97%, a multifunctional advantage not possessed by most single-purpose adsorbents. This unique property makes it more suitable for integrated scenarios of "wastewater treatment + waste gas purification" in printing and dyeing workshops, thereby expanding its practical application value.

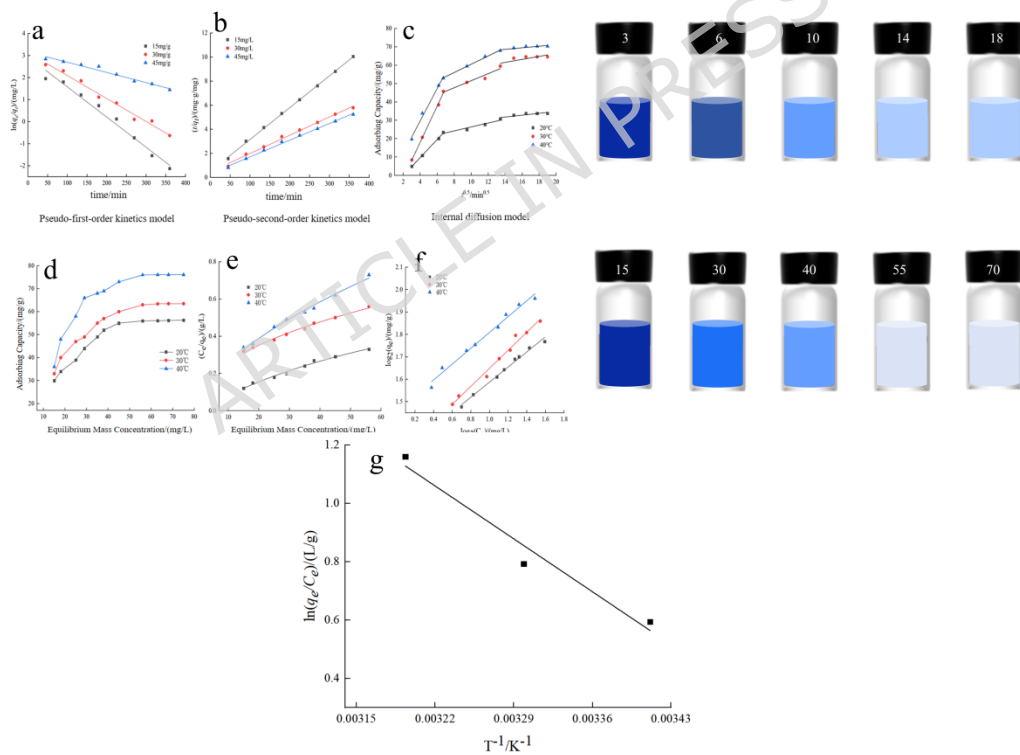


**Fig. 7.** (a ) (b) (c) Adsorption Kinetic Model. (d) (e) (f) Adsorption isotherm model diagram. (g) Van Tehoff Diagram.

**Table 5.** Adsorption Kinetic Parameters.

$C_0/(mg/g)$	Pseudo-first-order kinetics model	Pseudo-second-order kinetics
--------------	-----------------------------------	------------------------------

L)	model						
	$q_e/(mg/g)$	$q_t/(mg/g)$	$k_1/mi\text{ }n^{-1}$	$R^2$	$q_v/(mg/g)$	$k_2/(g\cdot mg^{-1}mi\text{ }n^{-1})$	$R^2$
15	36.968	33.447	0.013	0.97	33.501	0.0264	0.99
	5	8	7	55	6		92
30	66.873	61.297	0.010	0.98	55.033	0.0152	0.99
	2	0	4	27	0		30
45	72.696	62.711	0.004	0.96	62.708	0.0139	0.99
	7	3	6	52	6		52

**Table 6.** Internal Diffusion Parameter.

temperature/°C	Surface diffusion		Mesopore diffusion		Micropore diffusion	
	$K_1/(mg/(g\cdot min^{0.5}))$	$R^2$	$K_2/(mg/(g\cdot min^{0.5}))$	$R^2$	$K_3/(mg/(g\cdot min^{0.5}))$	$R^2$
20	4.9390	0.9975	1.0705	0.950	0.5120	0.6677
30	9.8470	0.9976	1.9190	0.9102	0.8145	0.5385
40	8.8055	0.9876	2.2565	0.94945	0.4259	0.7020

**Table 7.** Adsorption Isotherm Parameters.

temperature/°C	Langmuir Model			Freundlich Model		
	$b/(L/mg)$	$q_m/(mg/g)$	$R^2$	$K_F/(mg/g)/(mg/L)^{1/n}$	$n$	$R^2$
						$K_F$
20	0.0102	56.1623	0.9849	17.8262	2.9690	0.9881
30	0.0049	63.4967	0.9887	17.6547	2.4839	0.9813
40	0.0016	76.0915	0.9879	28.5817	2.8297	0.9818

**Table 8.** Adsorption Thermodynamic Parameters.

temperature/°C	$\Delta G/(kJ/mol)$	$\Delta S/(J/mol\cdot K)$	$\Delta H/(kJ/mol)$

	(kJ·mol <sup>-1</sup> )	(J·mol <sup>-1</sup> ·K <sup>-1</sup> )	(kJ·mol <sup>-1</sup> )
20	-1.4491		
30	-1.9995	87.5441	24.1223
40	-3.0223		

## 4. Conclusions

Hemp was dissolved in LiCl/DMAc to prepare a cellulose solution, which was blended with PAN for electrospinning. Single-factor experiments optimized the process, yielding a fiber membrane with smooth morphology, good fiber orientation, and cellulose I crystalline structure. Elemental analysis showed effective blending, with increased C and O contents compared to pure PAN. A Box-Behnken Design (BBD) was used to investigate dye adsorption factors, establishing a well-fitting regression model. Under optimal conditions, the nanofiber membrane achieved a 95.05 % maximum dye adsorption rate. Its excellent properties suggest broad application prospects in various fields. It should be noted that this study employed a simulated wastewater system containing a single MB dye, and adsorption conditions such as pH were optimized specifically for this system. However, actual textile printing and dyeing wastewater has a complex composition, including multiple dyes, salts, surfactants, and other auxiliaries, which may interfere with the adsorption process of the composite fiber membrane. Therefore, future research can focus on the following directions: (1) Evaluate the adsorption performance of the membrane in multi-component dye systems or actual textile printing and dyeing wastewater to verify its applicability under complex water quality conditions; (2) Investigate the

anti-interference ability of the membrane against coexisting substances (such as inorganic salts, anionic surfactants, etc.) and clarify the influence mechanism of impurities on adsorption efficiency; (3) Examine the regeneration and reuse performance of the composite fiber membrane to reduce application costs and improve its economic feasibility. These extended studies will further enhance the practical application value of the hemp/PAN composite fiber membrane and provide more comprehensive technical support for its industrial application in the field of wastewater treatment.

## **CRediT authorship contribution statement**

Jiayi Wang: Writing - original draft, Validation  Data collection, results interpretation. Ying Sun: Writing - review & editing, Methodology, Funding acquisition. Weishuai Kong: Writing - review & editing, Supervision, Conceptualization. Yucan Jia: Investigation, Formal analysis. All authors: The conception and design of the study, or acquisition of data, or analysis and interpretation of data. Drafting the article or revising it critically for important intellectual content. Final approval of the version to be submitted.

## **Declaration of Competing Interest**

The authors declare that they have no known competing financial interests or personal relationships.

## **Funding**

This work was supported by the 2024 Heilongjiang Provincial Colleges and Universities Basic Scientific Research Business Fee Scientific Research Project (grant number: 145409703)

## Data Availability

All the data in this research are available upon reasonable request to the corresponding author.

## References

1. Li, W., Mu, B. N., Yang, Y. Q. Khalil-ur-Rehman, Feasibility of industrial-scale treatment of dye wastewater via bio-adsorption technology. *Bioresource Technology*. **277**, 157-170 (2019).
2. Mittersteiner, M., Schmitz, F., Barcellos, I. O. Reuse of dye-colored water post-treated with industrial waste: Its adsorption kinetics and evaluation of method efficiency in cotton fabric dyeing. *J. Water Process Eng.* **17**, 181-187 (2017).
3. Kraan, M. V. D., Cid, M. V. F., Woerlee, G. F., Veugelers, W. J. T., Witkamp, G. J. Dyeing of natural and synthetic textiles in supercritical carbon dioxide with disperse reactive dyes. *J. Supercrit. Fluids*. **40**, 470-476 (2007).
4. Liu, Z. C.; Khan, T. A.; Islam, M. A.; Tabrez, U. A review on the treatment of dyes in printing and dyeing wastewater by plant biomass carbon. *Bioresour. Technol.* **2022**, 354, 127168.  
<https://doi.org/10.1016/j.biortech.2022.127168>
5. Aarab, N. et al. Removal of an emerging pharmaceutical pollutant (metronidazole) using PPY-PANi copolymer: Kinetics, equilibrium and DFT identification of adsorption mechanism. *Groundw. Sustain. Dev.* **11**, 100416 (2020).

6. Ighalo, J. O. et al. Recent advances in hydrochar application for the adsorptive removal of wastewater pollutants. *Chem. Eng. Res. Des.* **184**, 419-456 (2022).
7. Al-Qahtani, S. D. et al. Synthesis and adsorption properties of fibrous-like aerogel from acylhydrazone polyviologen: Efficient removal of reactive dyes from wastewater. *J. Mater. Res. Technol.* **18**, 1822-1833 (2022).
8. Liu, Y. Q. et al. Environmental Impacts and Biological Technologies Toward Sustainable Treatment of Textile Dyeing Wastewater: A Review. *Sustainability* **16**(24), 10867 (2024).
9. Birniwa, A. H. et al. Adsorption Behavior of Methylene Blue Cationic Dye in Aqueous Solution Using Polypyrrole-Polyethylenimine Nano-Adsorbent. *Polymers* **14**(16), 3362 (2022).
10. Maponya, T. C., Makgopa, K., Somo, T. R., Modibane, K. D. Highlighting the Importance of Characterization Techniques Employed in Adsorption Using Metal-Organic Frameworks for Water Treatment. *Polymers* **14**(17), 3613 (2022).
11. Huang, X. M. et al. The Adsorption of Cd(II) on Manganese Oxide Investigated by Batch and Modeling Techniques. *Int. J. Environ. Res. Public Health* **14**(10), 1145 (2017).
12. Abdulhussain, R., Adebisi, A., Conway, B. R., Asare-Addo, K. Electrospun nanofibers: Exploring process parameters, polymer selection, and recent applications in pharmaceuticals and drug delivery. *J. Drug Delivery Sci. Technol.* **90**, 5133-5156 (2023).
13. Sopan, N., Namdeo, J., Pravin, G., Tejashwini, M. Pharmaceutical applications of electrospinning, *Ann. Pharm. Fr.* **78**(1), 1-11 (2020).
14. Li, H., Chen, X., Lu, W., Wang, J., Xu, Y., Guo, Y. Application of Electrospinning in Antibacterial Field, *Nanomaterials* **11**, 1822 (2021).
15. Cen, L. S. et al. Fabrication of ZIF-8/TiO<sub>2</sub> electrospinning nanofibers for

synergistic photodegradation in dyeing wastewater. *J. Ind. Eng. Chem.* **126**, 537-545 (2023).

16. Zhang, Y. R., Wang, Y. X. One-step electrospinning of cellulose acetate/chitosan/TiO<sub>2</sub> fibrous membranes: efficient humic acid removal by synergistic adsorption and photocatalysis. *Cellulose* **31**, 6815-6826 (2024).

17. Sreesha, M., Luke, L., Frederik, M.U., Jagannadh, S. Exploring hemp seed hull biomass for an integrated C-5 biorefinery: Xylose and activated carbon, *J. Bioresour. Bioprod.* **9**(3), 310-321 (2024).

18. Ma, H.W.; Cheng Z.Y.; Li, X.B.; Li, B.; Fu, Y.J.; Jiang, J.C. Advances and challenges of cellulose functional materials in sensors, *J. Bioresour. Bioprod.* **8**(1), 15-32(2023).

19. Zimniewska, M. Hemp Fibre Properties and Processing Target Textile: A Review. *Materials* **15**(5), 1901 (2022).

20. Deshmukh, G. S. Advancement in hemp fibre polymer composites: a comprehensive review. *J. Polym. Eng.* **42**(7), 575-598 (2022).

21. Karbownik, I., Rac-Rumijowska, O., Fiedot-Toboła, M., Rybicki, T., Teterycz, H. The Preparation and Characterization of Polyacrylonitrile-Polyaniline (PAN/PANI) Fibers. *Materials* **12**, 664 (2019).

22. Heinz, S., Gemmer, L., Janka, O., Gallei, M. Ferrocene-Modified Polyacrylonitrile-Containing Block Copolymers as Preceramic Materials. *Polymers* **16**(15), 2142 (2024).

23. Ahmad, M. et al. Effective Poly(Cyclotriphosphazene-Co-4,4'-Sulfonyldiphenol)@rGO Sheets for Tetracycline Adsorption: Fabrication, Characterization, Adsorption Kinetics and Thermodynamics. *Nanomaterials* **11**(6), 1540 (2021).

24. Noreen, S. et al. Original ZnO, MgO and FeO adsorption efficiencies for direct sky Blue dye: equilibrium, kinetics and thermodynamics studies. *Journal of Materials Research and Technology* **9**(3), 5881-5893 (2020).

25. Li, Z. Y. et al. Kinetics and thermodynamics of NPX adsorption by  $\gamma$ -FeOOH in aqueous media. *Arabian Journal of Chemistry* **11**(6), 910-917 (2018).

26. Zhang, H. Y., Li, A. M., Sun, J., Li, P. H. Adsorption of amphoteric aromatic compounds by hyper-cross-linked resins with amino groups and sulfonic groups. *Chem. Eng. J.* **217**, 354-362 (2013).

27. Gao, Z. P., Yu, Z. F., Yue, T. L., Quek, S. Y. Adsorption isotherm, thermodynamics and kinetics studies of polyphenols separation from kiwifruit juice using adsorbent resin. *J. Food Eng.* **116**(1), 195-201 (2013).

28. Song, Y. J. et al. Droplet Spreading Characteristics on Ultra-Slippery Solid Hydrophilic Surfaces with Ultra-Low Contact Angle Hysteresis. *Coatings* **12**(6), 755 (2022).

29. Thao, D. V., Dung, T. N., Huy, N. N. Efficient Rhodamine B removal by photocatalysis using polyacrylonitrile/ $\text{Ag}_2\text{S}$  nanofibers prepared by combining electrospinning technology and facile gas-solid reaction. *Vietnam J. Chem.* **62**, 269-279 (2024).

30. Jiang, J. J. et al. Superfast, large-scale harvesting of cellulose molecules via ethanol pre-swelling engineering of natural fibers. *Carbohydr. Polym.* **343**, 2473-2484 (2024).

31. Freitas, G. P. et al. Starch-based films: Tuning physical properties driven by nanocellulose-natural rubber latex composites. *Ind. Crops Prod.* **221**, 9364-9375 (2024).

32. Birlie, B., Mamay, T. Characterization of natural cellulosic fiber extracted from *Grewia ferruginea* plant stem. *Int. J. Biol. Macromol.* **27**(2), 132847-132858 (2024).

33. Yang, Z. X.; et al. Characterization and value-added applications of natural cellulose fibers derived from cow dung in cementitious composites. *Cellulose* **31**(9), 5575-5589 (2024).

34. Ghoul, Y. E., Altuwayjiri, A. S., Alharbi, G. A. Synthesis and characterization of new electrospun medical scaffold-based modified cellulose nanofiber and bioactive natural propolis for potential wound dressing applications. *RSC Adv.* **14**(36), 26183-26197 (2024).

35. Shibly, M. A. H. et al. Hylocereus undatus plant's stem agro-waste: A potential source of natural cellulosic fiber for polymer composites. *Sustain. Chem. Pharm.* **41**, 1681-1692 (2024).

36. Fu, J. X. et al. Preparation of a locust protein and cellulose composite as natural based source material for air filtration membrane fabrication. *Polymer* **308**, 7342-7353 (2024).

37. Chen, J. H. et al. Natural lignocellulosic biomass structure inspired CNF/Lignin/PBAT composite film with thermoplastic, antibacterial and UV-blocking abilities. *Int. J. Biol. Macromol.* **271**(1), 132487-132498 (2024).

38. Zhou, H. L., Jin, W. Q. Membranes with Intrinsic Micro-Porosity: Structure, Solubility, and Applications. *Membranes* **9**(1), 3 (2019).

39. Lo, C.-F., Yu, C.-Y., Kuan, I.-C., Lee, S.-L. Optimization of Lipase Production by Burkholderia sp. Using Response Surface Methodology. *Int. J. Mol. Sci.* **13**, 14889-14897 (2012).

40. Li, Z. H., Zhang, S. H., Zhu, G. A., Xing, J. Use of graphene oxide for the removal of norfloxacin and ceftriaxone antibiotics from aqueous solution: process optimization using response surface approach. *Front. Environ. Sci.* **12**, 6837-6848 (2024).

41. Kara, A., Demirbel, E. Kinetic, Isotherm and Thermodynamic Analysis on Adsorption of Cr(VI) Ions from Aqueous Solutions by Synthesis and Characterization of Magnetic-Poly(divinylbenzene-vinylimidazole) Microbeads, *Water Air Soil Pollut* **223**(5), 2387-2403 (2012).

42. Zhao, H. J. et al. Unveiling the adsorption mechanisms of macrolides by mesoporous carbons through molecular dynamics simulation and multilinear

regression modelling. *Sep. Purif. Technol.* **353**(C), 8468-8479 (2025).

43. Xiao, S. H. et al. Adsorption and Diffusion Properties of Gas in Nanopores of Kerogen: Insights from Grand Canonical Monte Carlo and Molecular Dynamics Simulations. *Processes* **12** (7), 1427-1438 (2024).

44. Emara, A. M.; Elsharma, E. M.; Abdelmonem, I. M. Adsorption of ytterbium(III) ions on ivy leaves marc: isotherm, kinetic and thermodynamic studies. *J. Radioanal. Nucl. Chem.* **334**(1), 227-237 (2025).

45. Dietenberger, M. A., Glass, S. V., Boardman, C. R. Comprehensive Analytical Sorption Thermodynamic (CAST) model for water vapor sorption in cellulosic materials. *Adsorption* **30** (6), 1251-1271 (2024).

46. Pelton, R. H., Karami, A., Mirabal, J. M. Analysis of polydisperse polymer adsorption on porous cellulose fibers. *Nordic Pulp & Paper Research Journal* **39**(3), 375-387 (2024).

47. Denisov, A. M.; Zhu, D. Q. Iterative Numerical Methods for Solving the Problem of Determining the Coefficient in the Sorption Dynamics Model. *Comput. Math. Math. Phys.* **64**(11), 2696-2704 (2024).

48. Gago, D., Chagas, R., Ferreira, L. M., Velizarov, S., Coelhoso, I. A Novel Cellulose-Based Polymer for Efficient Removal of Methylene Blue. *Membranes* **10**(1), 13 (2020).

49. Al Othman, Z. A.; Hashem, A.; Habila, M. A. Kinetic, equilibrium and thermodynamic studies of cadmium (II) adsorption by modified agricultural wastes. *Molecules* **16**(12), 10443-10456 (2011).

50. Li, R. S., Xie, Z. J., Zhou, Y., Wang, W. L., Gui, X. H. Investigation of synergistic mechanism of magnesium ions and cationic surfactant in low-rank coal flotation. *Comput. Math. Math. Phys.* **137**, 280-292 (2024).

51. Bhagawati, P. B., Adeogun, A. I., Shivayogimath, C. B., Kadier, A. Gum Arabic tree biomass derived activated carbon for fluoride sequestration in batch and fixed bed processes: kinetics, thermodynamics and column

adsorption modeling. *J. Dispersion Sci. Technol.* **46**(4), 619-627 (2025).

52. Kong, L.J., Zhang, M.Y. Adsorption of Methylene Blue on Chestnut Shell-Based Activated Carbon: Calculation of Thermodynamic Parameters for Solid-Liquid Interface Adsorption. *Catalysts* **12**(8), 813 (2022).

53. Wang, Y., Huang, J., Zhang, Y., Zhang, S., Li, L., Pang, X. The Design of PAN-Based Janus Membrane with Adjustable Asymmetric Wettability in Wastewater Purification. *Materials* **17**(2), 417 (2024).

54. Jian, S.J., Wu, J.L., Ran, L., Yang, W.S., Duan, G.G., Yang, H.Q., Shi, F.S., Chen, Y.H., Hu, J.P., Jiang, S.H. Electrospun nanofibers membranes of La(OH)<sub>3</sub>/PAN as a versatile adsorbent for fluoride remediation: Performance and mechanisms. *E-Polymers* **24**(1), 20240083 (2024).